water

MDPI

Article

# Decline of N and P Uptake in the Inner Protection Zone of a Terminal Reservoir during Inter-Basin Water Transfers

**Shengtian Yang [1], Juan Bai [2,3], Changsen Zhao [1], Hezhen Lou [1,*], Zhiwei Wang [2,4], Yabing Guan [2], Yichi Zhang [2], Chunbin Zhang [2] and Xinyi Yu [2]**

1 College of Water Sciences, Beijing Normal University, Beijing 100875, China; yangshengtian@bnu.edu.cn (S.Y.); hzjohnson@gmail.com (C.Z.)
2 State Key Laboratory of Remote Sensing Science, Faculty of Geographical Science, Beijing Normal University, Beijing Key Laboratory for Remote Sensing of Environment and Digital Cities, Beijing 100875, China; baijuanaction@163.com (J.B.); wangzhiweisci@gmail.com (Z.W.); guanyabing2013@163.com (Y.G.); yichizhang@mail.bnu.edu.cn (Y.Z.); zhangchunbin1102@163.com (C.Z.); yuxy0106@sina.com (X.Y.)
3 College of Geographical Science, Shanxi Normal University, Linfen 041004, China
4 Key Laboratory of Radiometric Calibration and Validation for Environmental Satellites, National Satellite Meteorological Center, China Meteorological Administration, Beijing 100081, China
* Correspondence: louhezhenbj@163.com; Tel.: +86-10-5880-5034

Received: 23 December 2017; Accepted: 6 February 2018; Published: 9 February 2018

**Abstract:** Inter-basin water transfer projects are designed to relieve water scarcity around the world. However, ecological problems relating to reductions in protection zone functions can occur during inter-basin transfers. This paper uses the largest inter-basin water transfer project in the world, namely, the South-to-North Water Transfer Project (SNWTP) in China, as an example to analyze the variation of Miyun Reservoir's inner protection zone functions when water is transferred. Specifically, a riparian model (RIPAM) coupled with remote sensing data were used to calculate the nitrogen (N) and phosphorus (P) losses due to plant uptake, and these results were validated by in situ survey data. Then, correlations between water levels and N and P removal were analyzed. The results show that water table disturbances resulting from elevated water levels strongly influence the growth of plants and have obvious negative impacts on N and P removal in the inner protection zone. With the implementation of the middle route of the SNWTP, the water level of Miyun will rise to 150 m in 2020, and subsequently, the total net primary productivity (NPP) could decline by more than 40.90% from the level in 2015, while the N and P uptake could decline by more than 53.03% and 43.49%, respectively, from the levels in 2015, according to the modeling results. This will lead to declines in the inner protection zone's defense effectiveness for N and P interception and increases in risks to the security of water resources. The results of this study provide useful knowledge for managing the defense function of the terminal reservoir's inner protection zone and for ensuring that water quality is maintained during the diversion process.

**Keywords:** protection zone; nutrient uptake; NPP; South-to-North Water Transfer Project; Miyun Reservoir

## 1. Introduction

Inter-basin water transfers can relieve water scarcity and are a popular water-resource topic. To date, many famous projects have been built to alleviate uneven water resource distributions, such as the Central Arizona Project, the Colorado River Projects and California North-to-South Water Transfer Project in the United States [1,2], the Siberian Rivers Diversion in Russia [3], the Snowy Mountains Scheme in Australia [4], the National River Linking Project in India [5], and the South-to-North Water Transfer Project (SNWTP) in China [6]. However, inter-basin water transfers usually are associated

with complex environmental changes [7–11], just as Davies et al. [7] proposed: "Any transfer of water within or between basins will have physical, chemical, hydrological and biological implications for both donor and recipient systems, as well as for their estuaries and local marine environments." Therefore, the environmental responses to inter-basin water transfers should be studied.

Numerous ecological changes during inter-basin water transfers have been proposed, including the introduction of nonindigenous species, secondary salinization, disturbances in water chemistry and quality, changes in hydrologic regimes, and alterations of habitats [8,11–18]. The major concerns of these studies were about the protection of water source regions and transfer canals so as to ensure water safety. However, more attention should be devoted to the problems faced in receiving areas of inter-basin water projects because artificial projects can raise the water level of a receiving area and flood its drinking water protection zones, which may result in a decline of surface water quality.

Drinking water protection zones have been established by law to maintain the quality of surface waters and aquatic ecosystems [19,20]. They consist of the following three parts: inner, middle, and outer protection zones [20]. The inner protection zone is located near the drinking water source, and its boundaries are closely related to the riparian buffer boundaries. The middle protection zone runs along the inner protection zone and covers certain buffer areas. The outer protection zone covers the remaining catchment area not covered by the inner protection zone and middle protection zone [19,20]. Among them, the inner protection zone is known for its ability to control non-point source pollution (NPS) by intercepting and retaining excess particulates and dissolved nutrients originating from the surrounding uplands. Plants in the inner protection zone play a significant role in nitrogen (N) and phosphorus (P) cycling, and they can reduce N and P concentrations in soils [21,22].

The absorption of nutrients by plants largely depends upon vegetation production and other environmental factors [23]. Even small changes in the water level may induce detectable changes in vegetation production and associated N and P removal efficiencies [24,25]. When an inter-basin water transfer project is implemented, significant amounts of water will be diverted to the terminal reservoir. The elevated water level will flood the current riparian buffer, and a new one will form with a new vegetation circumstance. Such variations have the potential to render the riparian buffer ineffective at intercepting NPS and may change the inner protection zone from a nutrient sink into a nutrient source [26]. However, though studies on the responses of riparian vegetation to flooding have been done in natural lakes and rivers with some success [27,28], the impacts of inter-basin water transfers on the N and P uptake functions of a terminal reservoir's protection zone have not yet been investigated.

In this study, we use the SNWTP in China, which is the largest inter-basin transfer project in the world, as an example to assess the impacts of water transfers on N and P uptake in a terminal reservoir's inner protection zone. The total N and P losses due to plant uptake were calculated by the combined use of an N and P model and remote sensing data, and then, the relationship between the water level and N and P removal was examined. Finally, the potential risks posed by water level fluctuations and associated impacts on N and P uptake in the inner protection zone were evaluated.

## 2. Materials and Methods

### *2.1. Study Area*

The SNWTP in China consists of three routes (i.e., the eastern, middle, and western routes) (Figure 1); each route covers a distance of more than 1000 km, and in total they deliver 44.8 billion $m^3$ of fresh water per year to northern China. It is the largest inter-basin transfer scheme in the world; therefore, it is often taken as an example of inter-basin transfers and has been intensively studied in terms of the ecological and environmental consequences since it was proposed [12,13,29–34].

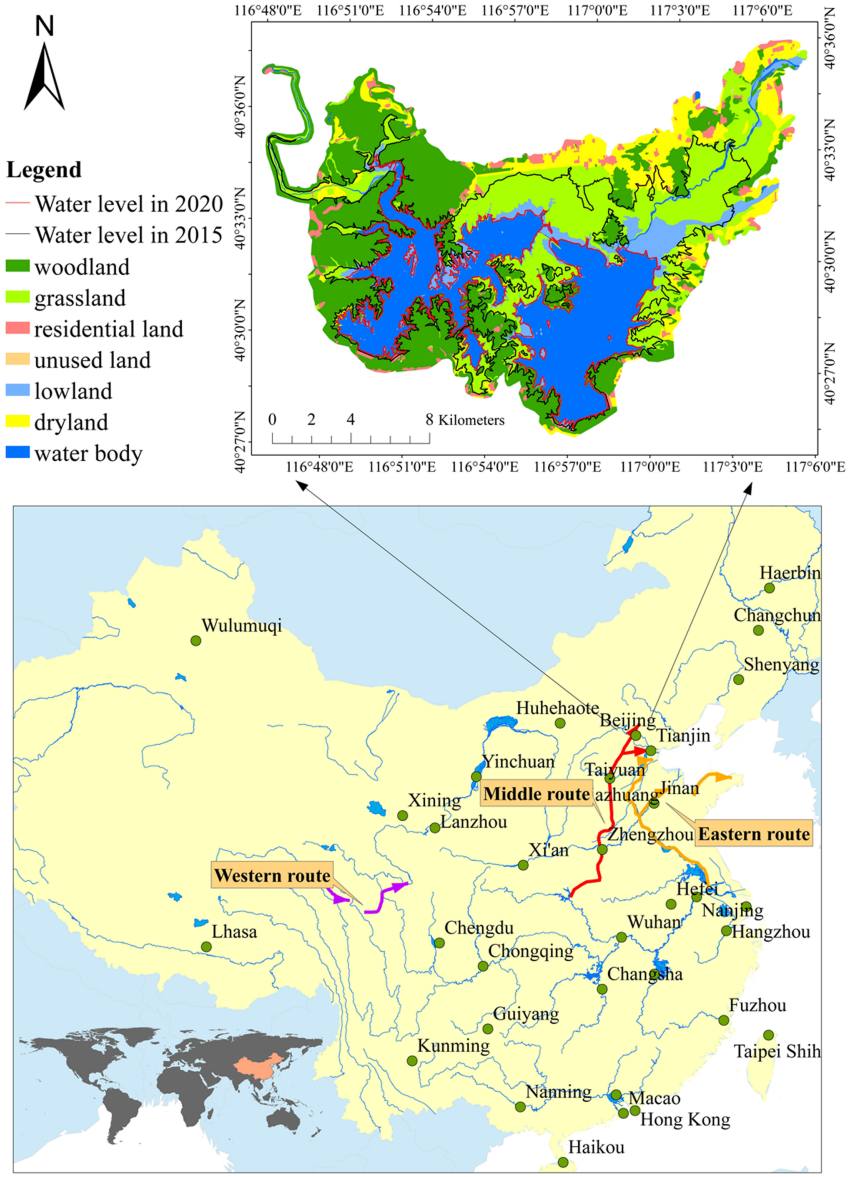


**Figure 1.** Schema of the South-to-North Water Transfer Project in China and land use information for the terminal Miyun Reservoir of the middle route.

Along the middle route, the Miyun Reservoir serves as the terminal point and stores surplus water transferred from the Dangjiangkou Reservoir. The middle route of the SNWTP was implemented in 2014. Surplus water is lifted 133 m in elevation so that it can enter the Miyun Reservoir through the Jingmi diversion canal with the help of nine pumping stations. The Miyun Reservoir is situated in the mountainous area of Miyun County, and the reservoir extends from 116°47′ E to 117°05′ E and from 40°26′ N to 40°35′ N (Figure 1). It has a large water surface area of 188 km$^2$ and a watershed area of 15,788 km$^2$; the total storage capacity is 4.375 billion m$^3$. The study area features a temperate continental monsoon climate, with a mean annual precipitation amount of 628 mm and mean annual air temperature of 11.3 °C. There is an uneven seasonal distribution of precipitation, and more than 70% of the annual precipitation occurs between June and September. The main land use types are dry land, woodland, grassland, water bodies, flood land, and residential land (Figure 1). The inner protection zone along the Miyun Reservoir mainly consists of the area encompassed by the highway surrounding the reservoir and other nearby water zones as designated by the government.

The Miyun Reservoir is the main surface drinking water source for Beijing, and it has played an important role in the social and economic development of the capital [35]. Issues related to water quality in the reservoir have been receiving increasing attention. The upper catchment of the Miyun Reservoir has exhibited eutrophication trends in recent years [36]. Thus, there is an urgent need to strengthen the management of water protection zones. The water level of the Miyun Reservoir was 136 m in 2016. With the implementation of the middle route of the SNWTP, the capacity of the terminal reservoir will be increased from 1.2 billion $m^3$ to 2 billion $m^3$ in 2020, which will raise the water level to 150 m. The transferred water will inundate part of the original inner protection zone. Vegetation in the remaining part will likely be affected by the rising water level, and these changes could pose water quality risks for the terminal reservoir.

### 2.2. Simulation of N and P Uptake

The effects of water level variation on the inner protection zone's defense functions were evaluated through modeling the N and P removal of vegetation during five years (1999, 2000, 2009, 2010, and 2015). The Miyun Reservoir began to receive transferred water in 2015, so we chose 2015 as the current year. In the following years, its water level will increase to 150 m, which is almost equal to the water level in 1999; hence, we chose 1999 as the objective year for reference. Besides, the difference of water levels between 1999 and 2000 was quite significant (149 m in 1999 and 142 m in 2000), as well as the difference between 2009 and 2010 (137 m in 2009 and 134 m in 2010), so these years were chosen as typical years. N and P losses were calculated by coupling remote sensing data with a RIPArian Model (RIPAM, EcoHAT, Beijing, China). RIPAM couples simple process-based modules and remote sensing data to estimate soil denitrification rates, soil nitrogen emissions, phosphorus removed by soil erosion, and nitrogen and phosphorus removal by vegetation uptake [37–40]. The framework of RIPAM that relates to N and P uptake is shown in Figure 2, and its main functions and parameters are listed in Table 1.

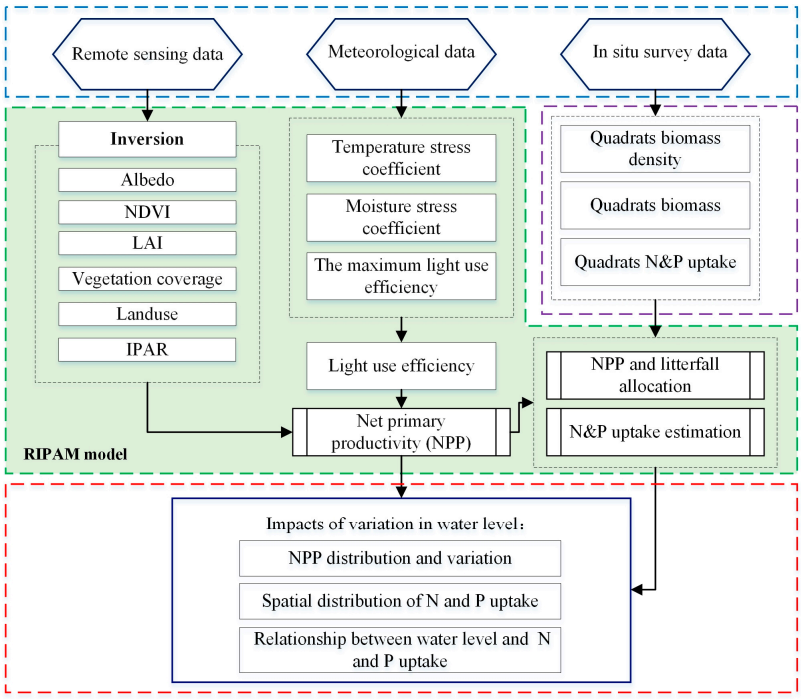


**Figure 2.** Framework of the N and P uptake simulation. IPAR: the amount of photosynthetically active radiation intercepted by plants; LAI: leaf area index; NPP: net primary productivity; NDVI: normalized difference vegetation index.

**Table 1.** Functions and parameters related to N and P uptake in the RIPAM model.

| No. | Module Name | Equations | Reference |
|---|---|---|---|
| 1 | NPP simulation | $NPP = GPP - R_a$<br>$GPP = \varepsilon \times IPAR \times f_1(T) \times f_2(\beta)$<br>$R_a = GPP \times (7.825 + 1.145T_a)/100$ | GLO-PEM model [41] |
| 2 | NPP allocation | $F_B = dB_L/d_t + dF_{lit}/d_t$<br>$B_L = LAI/SLA$<br>$R_B = K_{ra}(NPP - F_B)$<br>$W_B = NPP - F_B - R_B)$ | ForNBM model [42] |
| 3 | Nutrient absorption | $X_{uptake} = \min(X_{avail}, X_{dem})$<br>$X_{dem} = (1 - K_{retra}) \times folX \times F_B + X_W \times W_B + X_r \times R_B$<br>$X_{dem} = NPP \times X_{cont}$ | ForNBM model [42,43] |
| 4 | Litterfall decomposition | $F_{lit} = \begin{cases} a_{fh}F_B, T_{air} > T_{fall}, \text{deciduous species} \\ F_B, T_{air} < T_{fall}, \text{deciduous species} \\ a_{fs}F_B, \text{evergreen species} \end{cases}$ | ForNBM model [42] |

Annotation: NPP: net primary productivity (g C·m$^{-2}$); GPP: gross primary productivity (g C·m$^{-2}$); $R_a$: primary production for autotrophic respiration (g C·m$^{-2}$); IPAR: the amount of photosynthetically active radiation intercepted by plants (MJ·m$^{-2}$); $\varepsilon$: the real efficiency of radiation utilization (g C·MJ$^{-1}$); $f_1(T)$ is a function of temperature stress; $f_2(\beta)$ is a function of water stress; $F_B$: the NPP foliage obtains (g C·m$^{-2}$); $B_L$: the foliage biomass (g·m$^{-2}$); $F_{lit}$: the leaf litter (g C·m$^{-2}$); t: the time step (month); SLA: specific leaf area; $R_B$: the NPP roots obtain (g C·m$^{-2}$); $K_{ra}$: return coefficient of leaf nutrients, constant; $W_B$: the NPP wood obtains (g C·m$^{-2}$); $X_{uptake}$: the nutrient uptake rate (g·m$^{-2}$); $X_{avail}$: the amount of available nutrients (X = N or P) (g·m$^{-2}$); $X_{dem}$: the nutrients demanded by biomass growth (g·m$^{-2}$); $K_{retra}$: the dimensionless foliage nutrient re-translocation proportion (Kretra = 0.35 for this study); folX: the nutrient (X = N or P) concentration of the foliage (g·g$^{-1}$); $X_w$: the nutrient concentration of the wood (g·g$^{-1}$); Xr: the nutrient concentration of the roots (g·g$^{-1}$); $a_{fh}$: the coefficient for deciduous species; afs: the coefficient for evergreen species; $T_{air}$: air temperature (°C); and $T_{fall}$: the threshold temperature for deciduous species litter (°C).

In other published papers [37–40], the RIPAM model was tested in the Guanting Reservoir, and the simulations of net primary productivity (NPP), NPP allocation, and nutrient uptake all had considerable accuracy during the growing season (take N uptake rates for example, its $R^2$ value is 0.95). Since the Miyun Reservoir and Guanting Reservoir are located within a distance of less than 100 km and their geographical conditions and climate are similar [36,39], we adopted the model parameters of the Guanting Reservoir to apply to the Miyun Reservoir [37,39,44]. The database required included remote sensing data, meteorological data, and in situ survey data. Remote sensing data and meteorological data were used to drive the RIPAM model and simulate NPP and N and P uptake. In situ survey data were used to validate the simulation results. The relationship between water levels and N and P uptake in the inner protection zone were analyzed by implementing zonal statistics. Then the impacts of N and P uptake were evaluated due to rising water levels.

### *2.3. Multi-Source Data for Driving the RIPAM*

Input data for the RIPAM model included meteorological data, remote sensing data, and soil data (Table 2). (1) The daily meteorological data in July of 1999, 2000, 2009, 2010, and 2015 were collected from the national basic weather station at Miyun Reservoir; (2) The remote sensing data included Landsat data and Advanced Spaceborne Thermal Emission and Reflection Radiometer (ASTER)–Global Digital Elevation Model (GDEM) data. Five time series of Landsat images in July or August of 1999, 2000, 2009, 2010, and 2015 were collected to infer land surface parameters. ASTER–GDEM was used to calculate the contour map with intervals of 10 m, and the whole study area was zoned into the following four belts: 130–140 m, 140–150 m, 150–160 m, and 160–170 m; (3) Soil data were derived from the Second National Soil Survey results and field investigations in the study area. All data were reproduced at 30 m × 30 m spatial resolutions and projected to Albers by using the World Geodetic System-84 (WGS 84) datum. Some data were resolved by using ENVI4.8 (Harris Corporation, Melbourne, FL, USA), ArcGIS10.1 (Environmental Systems Research Institute, Redlands, CA, USA), or programs written in IDL (Interactive Data Language).

**Table 2.** Information for the multi-source data.

| Data Type | Data Name | Resolution | Data Source |
|---|---|---|---|
| Meteorological data | Precipitation, wind speed, air pressure, air temperature, daily max/min temperature, relative humidity, sunshine duration, sun radiation, surface temperature | - | National basic weather station (http://data.cma.cn/) |
| Remote sensing data | Digital elevation model (DEM) | 30 m | ASTER-GDEM (http://www.gscloud.cn/) |
| | Albedo, NDVI, LAI, land use, vegetation coverage, land surface temperature (LST) | 30 m | Landsat (http://www.gscloud.cn/) |
| Soil data | Bulk density, soil texture, soil nutrient content (TN, $NO_3$-N, $NH_4$-N), pH | - | Second National Soil Survey field investigations |

### *2.4. In Situ Survey Data for Validation*

In practice, biomass is seldom estimated over a large scale. In the present paper, biomass data in situ were collected at the times of Landsat image capture (from 5 to 20 July 2015) within the inner protection zone. The whole zone can be classified into the following three phases: reservoir, terrestrial, and water phase. The water phase is located between the low-water mark and the reservoir bank, the riparian phase contains the zone between the low-water mark and high-water mark, and the remainder is the terrestrial phase. Several 90 m × 90 m quadrants were selected in each phase, and Figure 3 shows some examples of the in situ quadrants. The location of each quadrant was recorded with the Global Positioning System (GPS) to integrate field and Landsat data. The harvesting method [45] was used to measure the average biomass density of grasses and shrubs. In each quadrant, we selected 36 sample areas of 1 m × 1 m for grass or nine sample areas of 5 m × 5 m for shrubs, and the average biomass density was calculated. Forest biomass was estimated using diameter–height models [46] based on the sample trees. In this study, 39 quadrants were selected for the analysis.

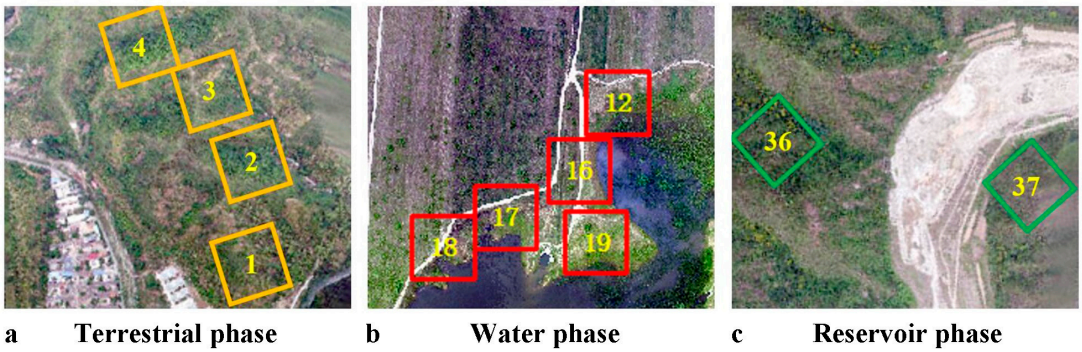


**Figure 3.** Examples of the in situ quadrants in different phases. (**a**) Quadrants selected in the terrestrial phase; (**b**) quadrants selected in the water phase; (**c**) quadrants selected in the reservoir phase.

The average biomass density of each quadrant was calculated, as shown in Table 3. Additionally, the data were converted into N and P uptake by using a simple ratio coefficient to validate the accuracy of the RIPAM model (see Section 3.4 for more details).

**Table 3.** Information for the biomass density of each quadrant. Quadrants 1–11 were selected in the terrestrial phase; quadrants 12–20 were selected in the water phase; quadrants 21–39 were selected in the reservoir phase.

| Quadrant ID | Biomass Density ($g \cdot m^{-2}$) | Quadrant ID | Biomass Density ($g \cdot m^{-2}$) | Quadrant ID | Biomass Density ($g \cdot m^{-2}$) |
|---|---|---|---|---|---|
| 1 | 1222.13 | 14 | 172.35 | 27 | 4699.23 |
| 2 | 1114.83 | 15 | 188.35 | 28 | 3139.40 |
| 3 | 773.61 | 16 | 171.57 | 29 | 4275.75 |
| 4 | 1321.03 | 17 | 192.58 | 30 | 13,825.23 |
| 5 | 1375.40 | 18 | 184.78 | 31 | 10,893.78 |
| 6 | 1185.17 | 19 | 177.98 | 32 | 7510.89 |
| 7 | 1332.65 | 20 | 142.32 | 33 | 12,186.66 |
| 8 | 1453.43 | 21 | 5291.21 | 34 | 10,159.57 |
| 9 | 859.52 | 22 | 3275.53 | 35 | 11,741.42 |
| 10 | 1001.63 | 23 | 1796.98 | 36 | 12,123.08 |
| 11 | 1488.09 | 24 | 2043.25 | 37 | 5930.64 |
| 12 | 172.73 | 25 | 1528.09 | 38 | 10,361.92 |
| 13 | 152.52 | 26 | 2679.09 | 39 | 7192.59 |

## 3. Results

### *3.1. NPP Distribution and Variation*

The NPP of Miyun's inner protection zone during the growing season of 1999, 2000, 2009, 2010, and 2015 was simulated by the RIPAM model. According to previous research in this study area [47], it is changes in water level but not climate or land use that influence the condition of vegetation in the inner protection zone. The total NPP of the whole zone amounted to 8454.96 t in 1999, 11,922.37 t in 2000, 17,271.43 t in 2009, 13,653.78 t in 2010, and 14,306.82 t in 2015. The spatial distribution and average NPP value during these five years are shown in Figure 4a–f. Higher values were mainly located in the northern part of the study area, where the values were more than 100 g $C \cdot m^{-2}$, while the NPP of the vegetation surrounding the reservoir was relatively low. The numerical growth of the NPP was significant in the northwestern and southwestern parts of the study area. As the water level rose, the average NPP value showed a decreasing trend, with values ranging from 98.66 g $C \cdot m^{-2}$ in 2015 at a water level of 133 m to 75.10 g $C \cdot m^{-2}$ in 1999 at a water level of 149 m (Figure 4f). The average water level in 2009, 2010, and 2015 was 135 m, and the average total NPP was 102.02 g $C \cdot m^{-2}$. The average water level in 1999 and 2000 was 145 m, and the corresponding average total NPP decreased to 83.40 g $C \cdot m^{-2}$, which amounts to a decline rate of 18.26%.

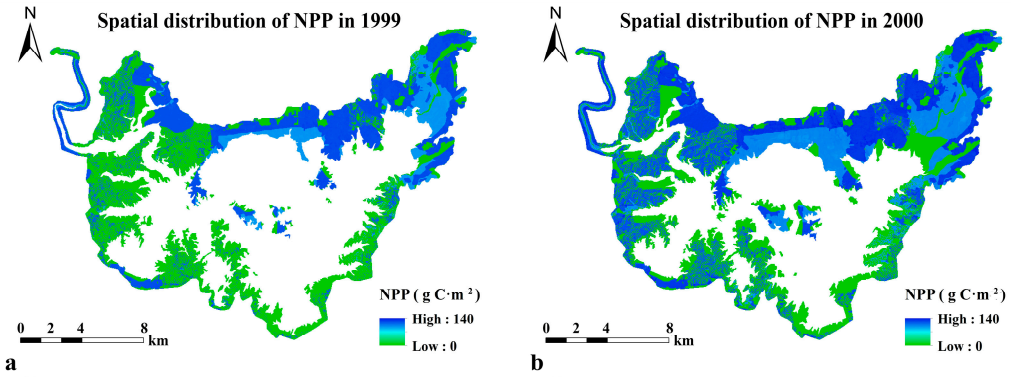


**Figure 4.** *Cont.*

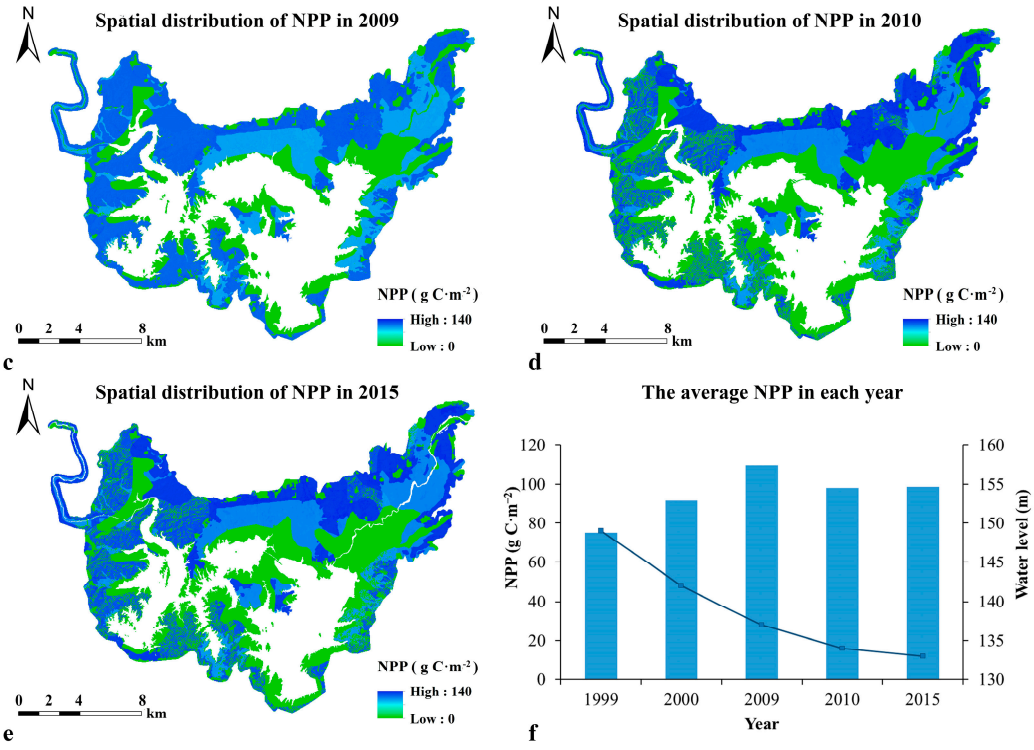


**Figure 4.** Spatial distribution of NPP in Miyun's inner protection zone during different years.

### *3.2. Spatiotemporal Variation of N and P Uptake*

The RIPAM model was used to simulate the spatial distribution of N and P uptake in the inner protection zone during the growing season of 1999, 2000, 2009, 2010, and 2015. Total N uptake of the whole zone amounted to 0.57 t in 1999, 0.74 t in 2000, 0.86 t in 2009, 0.78 t in 2010, and 1.22 t in 2015, while total P uptake of the whole zone amounted to 3.79 t in 1999, 5.93 t in 2000, 6.96 t in 2009, 6.33 t in 2010, and 6.71 t in 2015. The spatial distribution of N uptake for each year is shown in Figure 5a–e. The modeling results show that plants located in the western and northern parts of the study area had a stronger ability to absorb N; average monthly N uptake rates in the inner protection zone were around 2.62 $g \cdot m^{-2}$. The western part is mountainous, and the major land cover is forest. For the northern part, which has a vast area of grassland, N consumption by plants was relatively weaker, except for dry land, which had higher values. In addition, areas adjacent to the water body displayed a consistently low ability to consume N. The statistics in Figure 5f show that the average N removal due to plant uptake increased from 1999 to 2015. This result is consistent with the NPP data. The value of N consumed by plants increased from 1.80 $g \cdot m^{-2}$ in 1999 to 3.83 $g \cdot m^{-2}$ in 2015.

The spatial distribution of P uptake for each year is shown in Figure 6a–e. The results show that plants located in the northwestern, northeastern, and southwestern parts of the study area had a stronger ability to absorb P; average monthly P uptake rates in the inner protection zone were around 0.041 $g \cdot m^{-2}$. These three areas are all mountainous, and the major land cover is forest. For the northern part, which has a vast area of grassland, the ability of plants to consume P was relatively weaker. Also, areas adjacent to the water body displayed a consistently low ability to consume P. The statistics in Figure 6f show that average P removal due to plant uptake increased from 1999 to 2015. This result is consistent with the NPP and N uptake data. The value of P increased from 0.026 $g \cdot m^{-2}$ in 1999 to 0.046 $g \cdot m^{-2}$ in 2015.

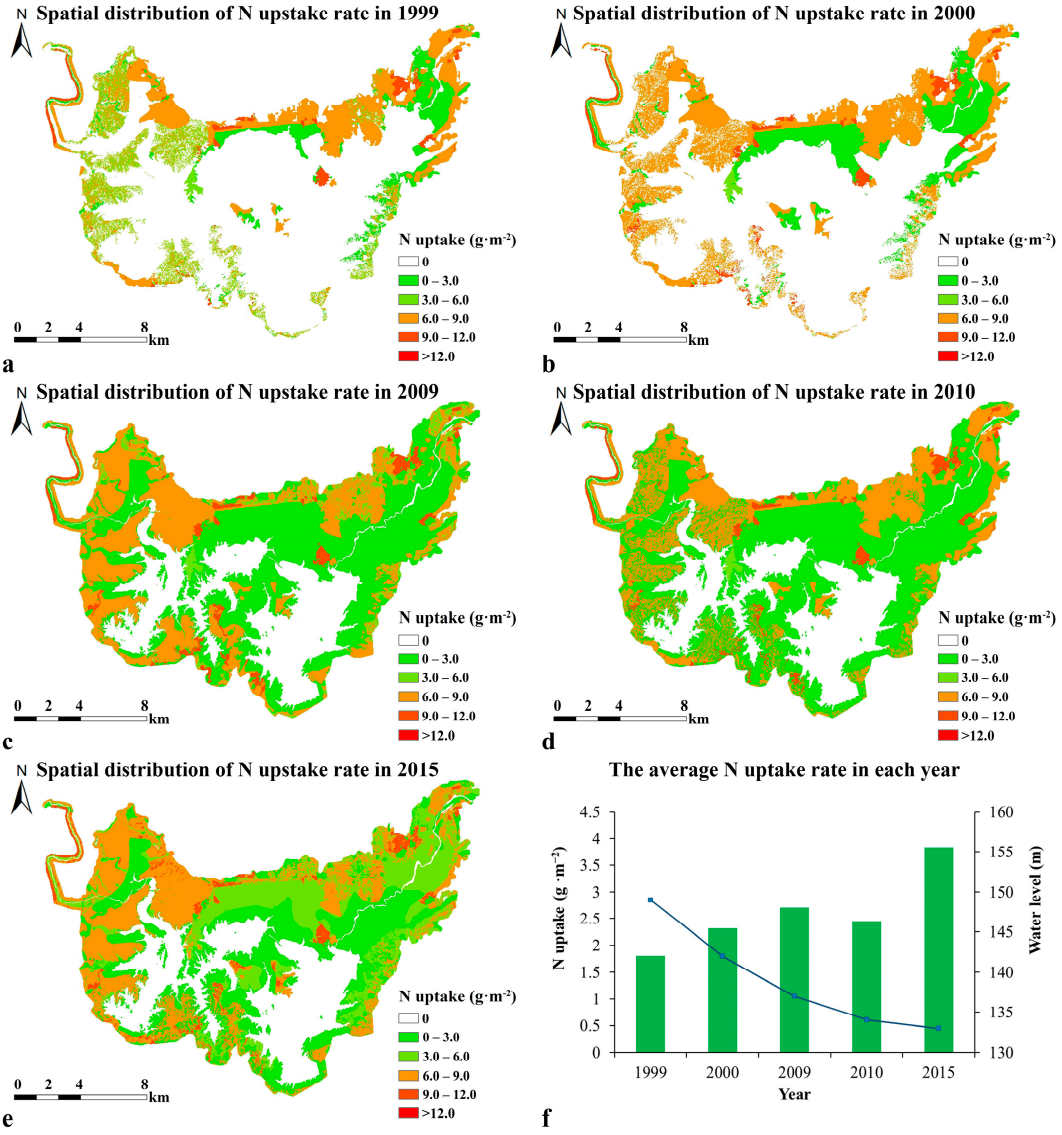


**Figure 5.** Spatial distribution of the N uptake rate in Miyun's inner protection zone during different years.

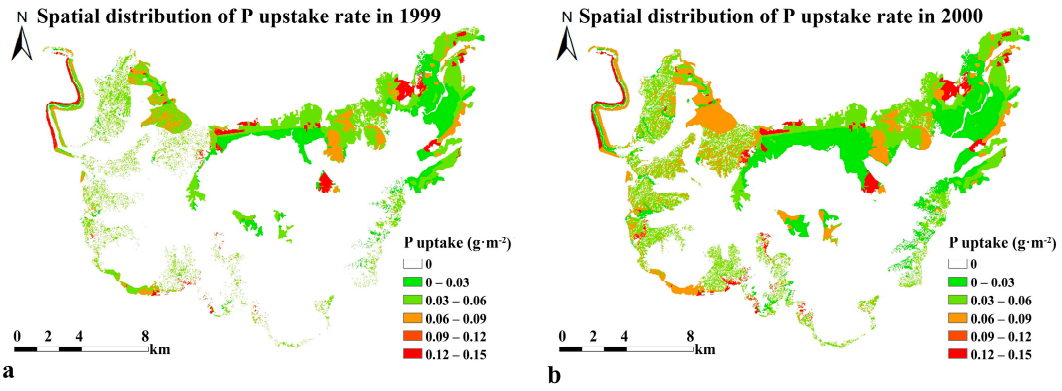


**Figure 6.** *Cont.*

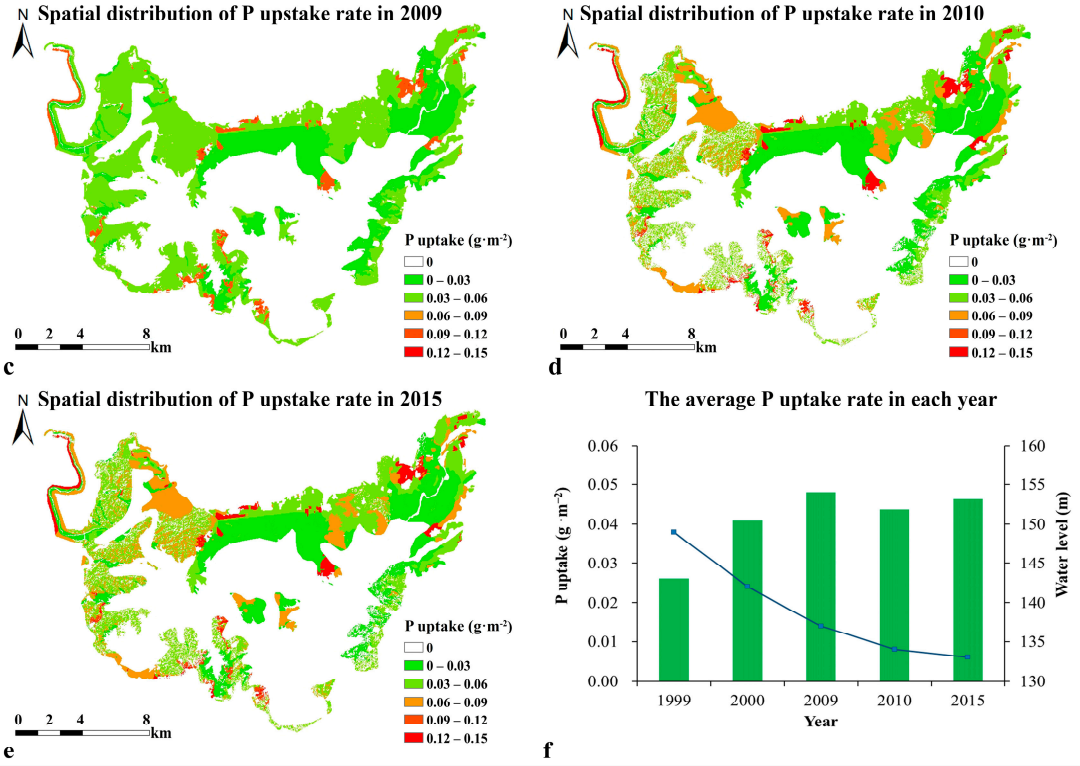


**Figure 6.** Spatial distribution of the P uptake rate in Miyun's inner protection zone during different years.

### *3.3. Negative Relationship between the Water Level and N and P Uptake*

Water table dynamics strongly influence the N and P removal rates by plants [25] in the inner protection zone and are impacted by both landscape and stream water levels directly [48]. By overlaying the contour map on the spatial distribution of N and P removal by plants and implementing zonal statistics (130–140 m, 140–150 m, 150–160 m, and 160–170 m), we found that the N and P uptake increased synchronously with the elevation gradient (Figure 7a,b). The mean N and P uptake were generally low between elevations of 130–160 m, where values for N varied from 16.44 t to 124.74 t and values for P varied from 16.44 t to 124.74 t. Meanwhile, the values were higher at 160–170 m, where the mean consumed N increased from 124.74 t to 427.20 t and the mean consumed P increased from 124.74 t to 427.20 t. Thus, the uptake of N and P by vegetation presented a positive correlation with elevation.

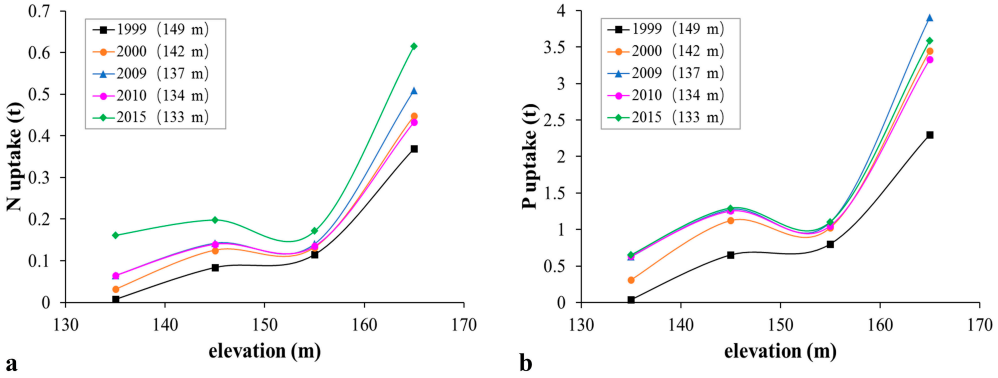


**Figure 7.** Zonal statistics for N (**a**) and P (**b**) consumed by plants during different years. The water level of each year is shown in parentheses following the year.

The amount of N and P removal by plants was also influenced by the water level. The lowest water level appeared in 2015, and the absorption of N and P by plants was strong in all elevation zones during this time. In 2009 and 2010, the water levels were similar, and the vegetation exhibited a similar N and P uptake capacity. The water level in 1999 was significantly higher than that in 2000, and the N and P uptake capacity of vegetation in 1999 was obviously lower than that of 2000. Thus, the increased water level had an obvious negative impact on N and P removal in the inner protection zone.

The response lines associating elevation with N and P uptake in Figure 7 can be classified into the following two categories based on the water level: high-level periods with an average water level of 145 m (1999, 2000) and low-level periods with an average water level of 134 m (2009, 2010, and 2015). The trend-line slopes of N and P uptake responses to different water levels are shown in Figure 8a,b. The slopes of N and P uptake during high-level periods were 0.145 and 0.0014, respectively, whereas they were 0.102 and 0.0009 during low-level periods, respectively. This shows that the N and P removal capacity of vegetation is more sensitive and weaker in high-level periods than in low-level periods. Therefore, the water levels of the reservoir along with the landscape have a significant impact on nutrient interception in the inner protection zone.

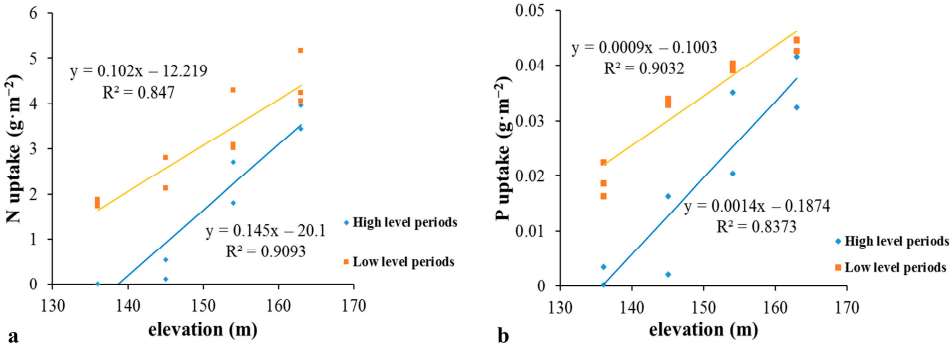


**Figure 8.** The distribution of N (**a**) and P (**b**) uptake rate responses to different water levels.

### *3.4. Validation of N and P Uptake Based on In Situ Survey Data*

Generally, there are correlations between vegetation biomass density and N and P uptake and biomass can be used as a surrogate for nutrient removal potential [49,50]. To validate the accuracy of the RIPAM model, we converted the biomass density to N and P uptake by using a simple ratio coefficient. Xiao [51] did research on the ratios between biomass and N and P uptake for woodland areas in the Miyun Reservoir watershed, and the average ratio between biomass and N uptake was 0.00487, while that between biomass and P was 0.000579 [51]. For grasslands, Song [52] found that the ratios between biomass and N and P uptake were 0.0152 and 0.0012, respectively [52]. In this study, 39 quadrants were selected (shown in Section 2.4), and the N and P uptake rate of each quadrant was obtained by multiplying the biomass density with the corresponding correlation as follows:

$$X_{uptake} = \text{Biomass} \times X_{rate}, \quad (1)$$

where $X_{uptake}$ refers to the N or P uptake rate of each quadrant ($g \cdot m^{-2}$), Biomass is the biomass density of each quadrant ($g \cdot m^{-2}$) (Table 3), and $X_{rate}$ is the ratio between the biomass and N and P uptake according to Xiao [50] and Song [51]. It should be noted that the $X_{rate}$ is varied with elevation and water level. Because of the limitation of the measured data, we used a fixed N or P uptake rate here and this would influence the results.

As each quadrant had a size of 90 m × 90 m, which corresponds to 3 pixels × 3 pixels in the RIPAM model, the average value of each 3 pixel × 3 pixel region in the simulated N and P uptake data was calculated. Then, scatter diagrams of N and P uptake between the RIPAM model and in situ quadrants were obtained, and linear regression was applied to the simulated data and in situ

survey data (Figure 9a,b). We found that the $R^2$ and relation coefficient for N uptake were 0.88 and 0.78, respectively; the $R^2$ and relation coefficient for P uptake were 0.82 and 0.6, respectively. Both were a good fit. This shows that the two simulations both had considerable accuracy.

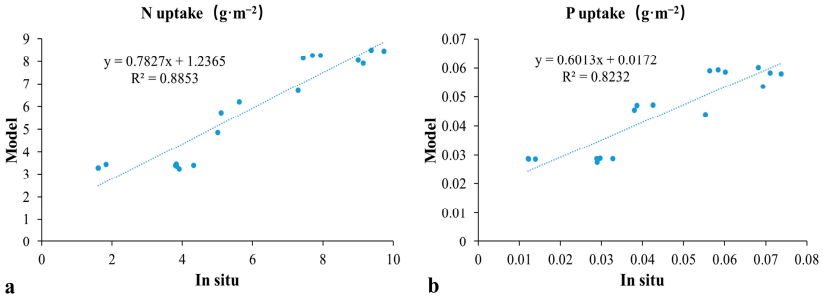


**Figure 9.** The N (**a**) and P (**b**) uptake rate of quadrant scatter diagrams between the RIPAM model and in situ survey.

## 4. Discussion

### *4.1. Reason for the Decline of N and P Uptake*

As mentioned in Section 3.3, water level dynamics can have obvious negative impacts on N and P uptake. The growth conditions are a primary influencing factor for nutrient uptake by plants. For vegetation in the inner protection zone, soil moisture is no longer a limiting factor to its growth. In high-water-level periods, prolonged inundation may cause mechanical injury to plants and adversely affect the growth of vegetation. Additionally, high soil moisture will have more inhibitory effects than stimulatory effects on vegetation development. These both will lead to low NPP [24,28].

According to the theory described above, NPP in the inner protection zone was evaluated zonally. It was found that the variation trend of NPP was similar with that of the N and P uptake by plants during the five years that were analyzed (Figure 10a,b). Generally, there was a rising trend in NPP with increasing altitude. The NPP increased slowly from 130 m to 150 m, with mean values varying from 149.43 t to 2780.30 t. At an altitude of 160 m, there was a decline in the NPP. Then, it rose exponentially from 160 m to 170 m, whereby the mean NPP increased from 2301.45 t to 6604.80 t. The NPP was also influenced by the water level. The mean NPP in each elevation zone was higher during the low water level years (corresponding to 2009, 2010, and 2015) than that during the high water level years (corresponding to 1999 and 2000). This can be explained by the differences in the vegetation distribution, which were driven largely by the tolerances of species to specific geomorphic processes. As shown in Figure 1, grasslands and dry lands are the dominant land use types at elevations of 130–160 m; they both are home to herbaceous species and are easily influenced by elevated water tables or flooding. Meanwhile, forests, which are the dominant land use type at 160–170 m, are less affected.

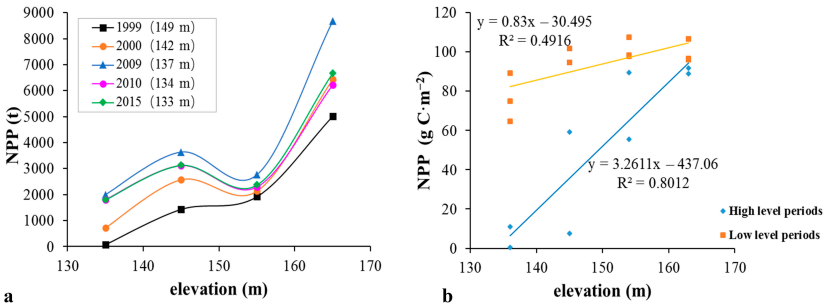


**Figure 10.** (**a**) Zonal statistics for NPP in different years and (**b**) NPP responses to different water levels. The numbers in parentheses following the years are the water level of each year.

### *4.2. Prediction of the Inner Protection Zone's Defense for N and P Interception*

With the implementation of the middle route of the SNWTP, the storage capacity of the Miyun Reservoir is expected to increase from 1 billion $m^3$ to 2 billion $m^3$, and the water level will rise to 150 m in 2020, which is higher than the level in 1999. According to the contour map, the extent of the inner protection zone will decrease to 122.23 $km^2$, which is less than 56% of the area in 2015, and changes will be especially prominent in the northern floodplain, which represents one of the most important sections that curtails N and P losses to the water source from the upstream watershed.

The rest of the zone will also be influenced by the elevated water tables. According to the formula in Figure 10b, NPP will decrease, especially for vegetation at elevations of 130–150 m, which is sensitive to flooding. The total NPP will likely be less than the amount of 8454.96 t detected in 1999 when the water level was 149 m, and it is predicted to decline by more than 40.90% compared to the level in 2015. According to the formulas in Figure 8a,b, N and P uptake will be less than the amounts of 0.57 t N and 3.79 t P detected in 1999, and each will decline by more than 53.03% and 43.49%, respectively, compared to the levels in 2015. Thus, the ecological functions of the original inner protection zone will be impaired and this will lead to a decline of the inner protection zone's defense effectiveness in terms of N and P interception.

Although some studies indicate that transferred water is safe and has little impact on the trophic state of the receiving water [14], its ecological effectiveness as a nutrient sink providing pollution control and sediment retention will be impacted if the extant inner protection zone is damaged. The inner protection zone may even be turned from an NPS sink to an NPS source [26]. This could pose risks to the security of the water resource. Thus, vegetation cover in the extant inner protection zone of the terminal reservoir will need to be restored if the protection zone is to maintain its usual effectiveness.

## 5. Conclusions

As the end point of the middle route of the South-to-North Water Transfer Project (SNWTP), the Miyun Reservoir is the most important water source for Beijing. Importantly, water quality in the reservoir can have a direct impact on the wellbeing of people in Beijing and therefore warrants protection. In particular, steps will need to be taken to avoid eutrophication problems. This study used the RIPAM model to simulate N and P uptake by plants in Miyun Reservoir's inner protection zone during five years (1999, 2000, 2009, 2010, and 2015), and the results were validated by in situ survey data ($R^2$ of N uptake was 0.88, and $R^2$ of P uptake was 0.82). The correlations between the water level and the N and P uptake capacities showed that water table dynamics strongly influence the N and P removal by plants; thus, variations in the water level can have obvious negative impacts on N and P removal in the inner protection zone.

With the implementation of the middle route of the SNWTP, the water level of the Miyun Reservoir will rise to 150 m in 2020, and the total NPP is predicted to decline by more than 40.90% compared to the level in 2015; additionally, the N and P uptake is predicted to decline by more than 53.03% and 43.49%, respectively, compared to the levels in 2015. This will lead to a decline in the inner protection zone's defense effectiveness in terms of N and P interception and pose risks to the security of the water resource unless steps are taken to avoid such negative consequences. In summary, this study provides useful knowledge for assessing the risks of nutrient removal reductions in a terminal reservoir from a large inter-basin water transfer project before its implementation.

**Acknowledgments:** We acknowledge all of the editors and reviewers for their valuable advice. The authors are thankful for A-Xing Zhu and Guiming Zhang in the Department of Geography at UW-Madison for their valuable advice. The authors are also thankful for the financial support from the National Natural Science Foundation of China (Grant Nos. U1603241, 51779099), the National Key Project for R&D (Nos. 2016YFC0402403, 2016YFC0402409), the project titled Impact of Rising Water Levels on the Riparian Ecological Environment in Miyun Reservoir (230200019), and the Central non-profit research institutes fundamental research of Yellow River Institute of Hydraulic Research (HKY-JBYW-2017-10).

**Author Contributions:** Shengtian Yang, Juan Bai and Zhiwei Wang conceived and designed the experiments; Juan Bai, Zhiwei Wang, Hezhen Lou, Chunbin Zhang, Yabing Guan and Xinyi Yu performed the experiments;

Shengtian Yang, Zhiwei Wang, and Hezhen Lou analyzed the data; Chunbin Zhang contributed analysis tools; Yichi Zhang prepared the figures; Shengtian Yang, Juan Bai, and Zhiwei Wang wrote the main manuscript text. All authors discussed the structure and commented on the manuscript at all stages.

**Conflicts of Interest:** The authors declare no conflict of interest. The founding sponsors had no role in the design of the study; in the collection, analyses, or interpretation of data; in the writing of the manuscript; and in the decision to publish the results.

## References


1. Cantor, L.M. The California state water project-a reassessment. *J. Geogr.* **1980**, *79*, 133–140.
2. Gastelum, J.R.; Cullom, C. Application of the Colorado River simulation system model to evaluate water shortage conditions in the central Arizona project. *Water Resour. Manag.* **2013**, *27*, 2369–2389. [CrossRef]
3. Voropaev, G.; Velikanov, A. Partial southward diversion of Northern and Siberian Rivers. *Int. J. Water Resour. Dev.* **1984**, *2*, 67–83. [CrossRef]
4. Hudson, J.W. *The Role of Water in the Biology of the Antelope Ground Squirrel Citellus Leucurus*; University of California Press: Berkeley, CA, USA, 1962.
5. Misra, A.K.; Saxena, A.; Yaduvanshi, M.; Mishra, A.; Bhadauriya, Y.; Thakur, A. Proposed river-linking project of India: A boon or bane to nature. *Environ. Geol.* **2007**, *51*, 1361–1376. [CrossRef]
6. Liu, C.; Zheng, H. South-to-North water transfer schemes for China. *Int. J. Water Resour. Dev.* **2002**, *18*, 453–471. [CrossRef]
7. Davies, B.R.; Thoms, M.; Meador, M. An assessment of the ecological impacts of inter-basin water transfers, and their threats to river basin integrity and conservation. *Aquat. Conserv.-Mar. Freshw. Ecosyst.* **1992**, *2*, 325–349. [CrossRef]
8. Yang, J.; Zhang, S.; Chang, L.; Li, F.; Li, T.; Gao, Y. Gully erosion regionalization of black soil area in Northeastern China. *Chin. Geogr. Sci.* **2017**, *27*, 78–87. [CrossRef]
9. Liu, K.; Ding, H.; Tang, G.; Na, J.; Huang, X.; Xue, Z.; Yang, X.; Li, F. Detection of catchment-scale gully-affected areas using unmanned aerial vehicle (uav) on the Chinese loess plateau. *ISPRS Int. J. Geo-Inf.* **2016**, *5*, 238. [CrossRef]
10. Zhuang, W. Eco-environmental impact of inter-basin water transfer projects: A review. *Environ. Sci. Pollut. Res. Int.* **2016**, *23*, 12867–12879. [CrossRef] [PubMed]
11. Li, Z.; Zhang, Y.; Zhu, Q.; Yang, S.; Li, H.; Ma, H. A gully erosion assessment model for the Chinese loess plateau based on changes in gully length and area. *Catena* **2017**, *148*, 195–203. [CrossRef]
12. Tang, C.; Yi, Y.; Yang, Z.; Cheng, X. Water pollution risk simulation and prediction in the main canal of the South-to-North water transfer project. *J. Hydrol.* **2014**, *519*, 2111–2120. [CrossRef]
13. Yang, W.; Zhang, L.; Shan, L.; Chen, X.; Chen, S. Response of extreme hydrological events to climate change in the water source area for the middle route of south-to-north water diversion project. *Adv. Meteorol.* **2016**, *2016*, 1–15. [CrossRef]
14. Zeng, Q.; Qin, L.; Li, X. The potential impact of an inter-basin water transfer project on nutrients (nitrogen and phosphorous) and chlorophyll a of the receiving water system. *Sci. Total Environ.* **2015**, *536*, 675–686. [CrossRef] [PubMed]
15. Zhang, Q. The South-to-North water transfer project of China: Environmental implications and monitoring strategy1. *J. Am. Water Resour. Assoc.* **2009**, *45*, 1238–1247. [CrossRef]
16. Zhang, Y.; Li, G.-M. Influence of south-to-north water diversion on major cones of depression in north China plain. *Environ. Earth Sci.* **2013**, *71*, 3845–3853. [CrossRef]
17. Li, Z.; Fang, H. Impacts of climate change on water erosion: A review. *Earth-Sci. Rev.* **2016**, *163*, 94–117. [CrossRef]
18. Pandey, A.; Himanshu, S.K.; Mishra, S.K.; Singh, V.P. Physically based soil erosion and sediment yield models revisited. *Catena* **2016**, *147*, 595–620. [CrossRef]
19. Walcher, M.; Bormann, H. On the transferability of the concept of drinking water protection zones from EU to Latin American Countries. *Water Resour. Manag.* **2015**, *29*, 1803–1822. [CrossRef]
20. Brenčič, M.; Prestor, J.; Kompare, B.; Matoz, H.; Kranjc, S. Integrated approach to delineation of drinking water protection zones. *Geologija* **2009**, *52*, 175–182. [CrossRef]

21. Sabater, S.; Butturini, A.; Clement, J.-C.; Burt, T.; Dowrick, D.; Hefting, M.; Matre, V.; Pinay, G.; Postolache, C.; Rzepecki, M. Nitrogen removal by riparian buffers along a European climatic gradient: Patterns and factors of variation. *Ecosystems* **2003**, *6*, 0020–0030. [CrossRef]
22. Correll, D. Buffer zones and water quality protection: General principles, Buffer zones: Their processes and potential in water protection. In Proceedings of the International Conference on Buffer Zones, Harpenden, Hertfordshire, UK, September 1996; pp. 7–20.
23. Klemas, V. Remote sensing of riparian and wetland buffers: An overview. *J. Coast. Res.* **2014**, *297*, 869–880. [CrossRef]
24. Nilsson, C.; Svedmark, M. Basic principles and ecological consequences of changing water regimes: Riparian plant communities. *Environ. Manag.* **2002**, *30*, 468–480. [CrossRef]
25. Liu, X.; Vidon, P.; Jacinthe, P.A.; Fisher, K.; Baker, M. Seasonal and geomorphic controls on n and P removal in riparian zones of the US Midwest. *Biogeochemistry* **2014**, *119*, 245–257. [CrossRef]
26. Schilling, K.E.; Li, Z.; Zhang, Y.-K. Groundwater–surface water interaction in the riparian zone of an incised channel, Walnut Creek, Iowa. *J. Hydrol.* **2006**, *327*, 140–150. [CrossRef]
27. Džubáková, K.; Molnar, P.; Schindler, K.; Trizna, M. Monitoring of riparian vegetation response to flood disturbances using terrestrial photography. *Hydrol. Earth Syst. Sci.* **2015**, *19*, 195–208. [CrossRef]
28. Kozlowski, T.T. Physiological-ecological impacts of flooding on riparian forest ecosystems. *Wetlands* **2002**. [CrossRef]
29. Stone, R.; Jia, H. Going against the flow. *Science* **2006**, *313*, 1034–1037. [CrossRef] [PubMed]
30. Zhang, J.; Meng, F.; Lu, Y.; Jing, Y.; Zhang, H.; Zhang, B.; Zhang, C. Ecological assessment of lakeshore wetland rehabilitation on eastern route of south-to-north water transfer project. *Front. Environ. Sci. Eng. China* **2008**, *2*, 306–310. [CrossRef]
31. Cheng, S.; Song, H. Conservation buffer systems for water quality security in south to north water transfer project in China: An approach review. *Front. For. China* **2009**, *4*, 394–401. [CrossRef]
32. Gu, W.; Shao, D.; Jiang, Y. Risk evaluation of water shortage in source area of middle route project for south-to-north water transfer in China. *Water Resour. Manag.* **2012**, *26*, 3479–3493. [CrossRef]
33. Liang, Y.-S.; Wang, W.; Li, H.-J.; Shen, X.-H.; Xu, Y.-L.; Dai, J.-R. The South-to-North water diversion project: Effect of the water diversion pattern on transmission of oncomelania hupensis, the intermediate host of *Schistosoma japonicum* in China. *Parasites Vectors* **2012**, *5*, 52. [CrossRef] [PubMed]
34. Barnett, J.; Rogers, S.; Webber, M.; Finlayson, B.; Wang, M. Sustainability: Transfer project cannot meet China's water needs. *Nature* **2015**, *527*, 295–297. [CrossRef] [PubMed]
35. Li, X.-S.; Wu, B.-F.; Zhang, L. Dynamic monitoring of soil erosion for upper stream of Miyun reservoir in the last 30 years. *J. Mt. Sci.* **2013**, *10*, 801–811. [CrossRef]
36. Jiao, J.; Du, P.; Lang, C. Nutrient concentrations and fluxes in the upper catchment of the Miyun reservoir, China, and potential nutrient reduction strategies. *Environ. Monit. Assess.* **2015**, *187*, 110. [CrossRef] [PubMed]
37. Dong, G.; Yang, S.; Gao, Y.; Bai, J.; Wang, X.; Zheng, D. Spatial evaluation of phosphorus retention in riparian zones using remote sensing data. *Environ. Earth Sci.* **2014**, *72*, 1643–1657. [CrossRef]
38. Wang, X.; Mannaerts, C.M.; Yang, S.; Gao, Y.; Zheng, D. Evaluation of soil nitrogen emissions from riparian zones coupling simple process-oriented models with remote sensing data. *Sci. Total Environ.* **2010**, *408*, 3310–3318. [CrossRef] [PubMed]
39. Wang, X.; Wang, Q.; Yang, S.; Zheng, D.; Wu, C.; Mannaerts, C.M. Evaluating nitrogen removal by vegetation uptake using satellite image time series in riparian catchments. *Sci. Total Environ.* **2011**, *409*, 2567–2576. [CrossRef] [PubMed]
40. Wang, X.; Yang, S.; Mannaerts, C.M.; Gao, Y.; Guo, J. Spatially explicit estimation of soil denitrification rates and land use effects in the riparian buffer zone of the large Guanting reservoir. *Geoderma* **2009**, *150*, 240–252. [CrossRef]
41. Prince, S.D.; Goward, S.N. Global primary production: A remote sensing approach. *J. Biogeogr.* **1995**, *22*, 815–835. [CrossRef]
42. Zhu, Z.X.; Arp, P.A.; Meng, F.R.; Bourque, C.P.A.; Foster, N.W. A forest nutrient cycling and biomass model (FORNBM) based on year-round, monthly weather conditions, part 1: Assumption, structure and processing. *Ecol. Model.* **2003**, *169*, 347–360. [CrossRef]
43. Arp, P.A.; Oja, T. A forest soil vegetation atmosphere model (ForSVA) 1. Concepts. *Ecol. Model.* **1997**, *95*, 211–224. [CrossRef]

44. Zhang, L.-T.; Li, Z.-B.; Wang, S.-S. Spatial scale effect on sediment dynamics in basin-wide floods within a typical agro-watershed: A case study in the hilly loess region of the Chinese loess plateau. *Sci. Total Environ.* **2016**, *572*, 476–486. [CrossRef] [PubMed]
45. Husson, E.; Lindgren, F.; Ecke, F. Assessing biomass and metal contents in riparian vegetation along a pollution gradient using an unmanned aircraft system. *Water Air Soil Pollut.* **2014**, *225*. [CrossRef]
46. Kachamba, D.J.; Orka, H.O.; Gobakken, T.; Eid, T.; Mwase, W. Biomass estimation using 3D data from unmanned aerial vehicle imagery in a tropical woodland. *Remote Sens.* **2016**, *8*, 968. [CrossRef]
47. Yang, S.; Bai, J.; Zhao, C.; Lou, H.; Zhang, C.; Guan, Y.; Zhang, Y.; Wang, Z.; Yu, X. The assessment of the changes of biomass and riparian buffer width in the terminal reservoir under the impact of the South-to-North water diversion project in China. *Ecol. Indic.* **2018**, *85*, 932–943. [CrossRef]
48. Jung, M.; Burt, T.; Bates, P. Toward a conceptual model of floodplain water table response. *Water Resour. Res.* **2004**, *40*. [CrossRef]
49. Rheinhardt, R.; Brinson, M.; Meyer, G.; Miller, K. Integrating forest biomass and distance from channel to develop an indicator of riparian condition. *Ecol. Indic.* **2012**, *23*, 46–55. [CrossRef]
50. Jiang, F.Y.; Chen, X.; Luo, A.C. A comparative study on the growth and nitrogen and phosphorus uptake characteristics of 15 wetland species. *Chem. Ecol.* **2011**, *27*, 263–272. [CrossRef]
51. Xiao, Y. Study on the Adjustment and Control Mechanism of Forest to Nonpoint Source Pollution in Beijing Mountain Area. Ph.D. Thesis, Beijing Forestry University, Beijing, China, 29 June 2008.
52. Song, X. Study on the Variation of N, P, K Nutrients Pool of Different Type of Alpine Meadow in Eastern Qilian Mountains. Master's Thesis, Gansu Agricultural University, Lanzhou, China, 10 June 2008.